Korean J. Chem. Eng., 40(12), 2957-2964 (2023)
DOI: 10.1007/s11814-023-1545-5

pISSN: 0256-1115
eISSN: 1975-7220

Efficient removal of hexavalent chromium (Cr(VI)) from wastewater using $FeCl_3$-modified *Chlorella*-based biochar

Soeun Moon*, Chang-Gu Lee*,†, Gwy-Am Shin*,†, and Seong-Jik Park**

*Department of Environmental and Safety Engineering, Ajou University, Suwon 16499, South Korea
**Department of Bioresources. and Rural System Engineering, Hankyong National University, Anseong 17579, South Korea
(*Received 29 June 2023 • Revised 3 August 2023 • Accepted 6 August 2023*)

Abstract−This study focuses on the adsorption of hexavalent chromium (Cr(VI)), a harmful heavy metal, using two types of *chlorella*-based biochar (biochar pyrolyzed at 200 °C (CB200) and iron chloride ($FeCl_3$)-modified biochar pyrolyzed at 200 °C (FeCB200)), and the testing of their effectiveness for the removal of Cr(VI). The FeCB200 sample exhibited the highest removal efficiency (1 g L^{-1}=66.12±1.01%; 5 g L^{-1}=98.48±0.22%) compared to raw biomass (1 g L^{-1}=54.05±0.00%; 5 g L^{-1}=90.09±0.26%) and CB200 (1 g L^{-1}=51.80±0.78%; 5 g L^{-1}=94.74±0.26%) in 100 mg L^{-1} Cr(VI) solution. The adsorbents were characterized using various characterization techniques, and adsorption experiments were carried out using varying doses of the adsorbent (1 and 5 g L^{-1}). Pseudo-second-order model provided the best fit for the adsorption kinetics, and Redlich-Peterson model exhibited good fitting for the adsorption isotherm (R^2>0.972), although variations were observed depending on the dose. Further, the applicability of FeCB200 was assessed using real wastewater spiked with Cr(VI). Although the presence of organic matter resulted in a reduction in the adsorption effectiveness of FeCB200, the difference was not significant (1 g L^{-1}=54.27±3.19%; 5 g L^{-1}=98.48±0.22%). These results demonstrate the promising potential of $FeCl_3$-modified *chlorella*-based biochar as a valuable adsorbent for the Cr(VI) removal from water environments.

Keywords: Adsorption, Biochar, *Chlorella*, Cr(VI), $FeCl_3$ Modification

INTRODUCTION

Various human activities, such as agricultural and industrial practices, contribute to the generation of wastewater contaminated with harmful heavy metals [1-3]. Among these heavy metals, hexavalent chromium (Cr(VI)) is of particular concern owing to its detrimental effects on both human health and the environment [4,5]. Exposure to Cr(VI) can lead to various detrimental health conditions in humans, including lung cancer, nasal and sinus cancers, kidney damage, liver problems, respiratory issues, and skin irritation [6,7]. Furthermore, its propensity for bioaccumulation in the food chain, non-biodegradable properties, and high carcinogenic nature can lead to severe environmental pollution [7,8]. Hence, it is crucial to reduce the presence of Cr(VI) in industrial/agricultural wastewater before it is discharged into public water bodies.

Different methods have been employed for the removal of Cr(VI) from wastewater, such as ion exchange [9], membrane filtration [10], photocatalytic reduction [3], and adsorption [11-13]. Particularly, the use of biochar-based adsorbents for Cr(VI) removal has emerged as an attractive method owing to its simplicity, cost-effectiveness, and wide applicability [14]. Biochar derived from various biomass sources, such as agricultural waste, wood chips, crop residues, and algae, possesses a highly porous structure and a large surface area, enabling efficient removal of heavy metals [15]. In addition, the stability of biochar ensures its suitability for long-term usage in water treatment applications [16]. The combination of these favorable physicochemical properties makes biochar a promising candidate for the Cr(VI) removal from polluted water sources, paving the way for sustainable and effective water treatment strategies.

Studies have demonstrated the great potential of microalgae as biomass due to its distinct characteristics, including exceptional adsorption capacity, environmental friendliness, and rapid growth rate [17,18]. *Chlorella*, one of the microalgae species, has attracted considerable attention in heavy metal adsorption studies. *Chlorella* possesses several advantageous features that enable its synergistic use with biochar. First, it exhibits a high affinity for heavy metals, enabling the efficient binding of metal ions [19]. Additionally, *chlorella* exhibits rapid growth rates and can be easily cultivated, making it a readily available and sustainable biomass [20]. Chemical activation can augment the adsorption capability of biochar. Chemical activation involves the treatment of biochar with activating agents like potassium hydroxide (KOH), phosphoric acid (H_3PO_4), zinc chloride ($ZnCl_2$), and iron chloride ($FeCl_3$), to increase its porosity and surface area [21]. In the context of studies on the adsorption of Cr(VI) through chemically modified biochar, one investigation employed H_3PO_4 activation on eucalyptus biochar, revealing that its efficiency in removing Cr(VI) surpassed that of non-modified eucalyptus biochar [22]. In another study, the adsorption performance of corn stover biochar towards Cr(VI) was assessed using distinct chemical activation methods ($ZnCl_2$ and $FeCl_3$). Notably, the biochar modified with both $ZnCl_2$ and $FeCl_3$ demonstrated the most elevated adsorption efficiency [23]. Among these agents,

†To whom correspondence should be addressed.
E-mail: changgu@ajou.ac.kr, gwyam@ajou.ac.kr
Copyright by The Korean Institute of Chemical Engineers.

$FeCl_3$ modification, used in this study, can enhance the adsorption capacity of Cr(VI) by increasing the surface polarity and specific surface area of biochar [24]. Nevertheless, further exploration of $FeCl_3$ modification on microalgae is still required.

Therefore, this study assessed the Cr(VI) adsorption behavior of *chlorella*-based biochar (with and without $FeCl_3$ modification). The main objectives of this research are as follows: (1) to compare the adsorption performance of raw biomass (CL), unmodified biochar (CB200), and $FeCl_3$-modified biochar (FeCB200), (2) to characterize FeCB200, which exhibits the highest adsorption performance, and (3) to assess the adsorption behavior of FeCB200 for Cr(VI), including investigations of the adsorption kinetics, isotherms, and its applicability in real wastewater.

MATERIAL AND METHODS

1. Chemicals and Materials

Chlorella sp. powder was obtained from Naturalmom (Seoul, Korea). Iron (III) chloride hexahydrate ($FeCl_3{\cdot}6H_2O$, ≥97.0%) was obtained from Duksan Chemicals (Ansan, Korea). Potassium dichromate ($K_2Cr_2O_7$, 99.5%), sym-diphenylcarbazide ($C_{13}H_{14}N_4O$), acetone (CH_3COCH_3, 99.5%), sodium hydroxide (NaOH, 98.0%), hydrochloric acid (HCl, 35.0-37.0%), and sulfuric acid (H_2SO_4, 95.0%) were provided from Samchun Chemical (Pyeongtaek, Korea).

2. Preparation of Adsorbents

Two types of *chlorella*-based adsorbents (biochar and $FeCl_3$-activated biochar) were prepared, and their Cr(VI)-adsorption performance was evaluated. Biochar is commonly produced by thermally decomposing biomass at temperatures ranging from 200 to 900 °C, a procedure recognized for its considerable energy demands and related expenses [25,26]. In this study, a lower pyrolysis temperature of 200 °C was selected, primarily influenced by economic considerations, to facilitate biochar production. To prepare the *chlorella*-based biochar (CB200), 10 g of *Chlorella* (CL) was subjected to pyrolysis in a furnace (FX-14, Daihan Scientific, Korea) (heating rate: 5 °C min^{-1}, temperature of 200 °C, duration: 2 h). To prepare the $FeCl_3$-activated *chlorella* biochar (FeCB200), 100 mL of 2 M $FeCl_3$ solution and 10 g of CL were stirred for 2 h. Thereafter, the solution was subjected to drying at 100 °C (duration: 2 h), and then pyrolyzed in a furnace (heating rate: 5 °C min^{-1}, temperature of 200 °C, duration: 2 h). The biochar obtained from pyrolysis was cleansed of impurities by rinsing with distilled water and subsequently dried at 100 °C using a vacuum oven (FTVO-701, SCI Finetech, Korea).

3. Characterization

The surface morphology of FeCB200 was characterized using field emission scanning electron microscopy (FE-SEM; JSM-7900F, JEOL, Japan) and field emission transmission electron microscopy (FE-TEM; Tecnai G2 F30 S-Twin, FEI, USA). The surface area of FeCB200 was determined via Brunauer-Emmett-Teller method (BET; Belsorp-max II, MicrotracBEL, Japan), and its pore size distribution was analyzed using N_2 adsorption-desorption experiment. The functional groups of FeCB200 were identified using Fourier transform infrared (FT-IR) spectroscopy (Nicolet iS50, Thermo Fisher Scientific, USA), while X-ray diffraction (XRD; Smartlab, Rigaku, Japan) was employed to analyze its crystalline minerals. The pH of the final effluent from the wastewater treatment plant was analyzed using a pH meter (Orion Star A211, Thermo Fisher Scientific, USA) and the dissolved organic carbon was measured via a TOC analyzer (TOC-Vws, Shimadzu, Japan). UV_{254} was measured at a wavelength of 254 nm using a UV-vis spectrophotometer (NEO-S2117, NEOGEN, Korea).

4. Adsorption Experiments

The Cr(VI) solutions used in this study were prepared via diluting the 1,000 mg L^{-1} Cr(VI) stock solution. To investigate the effect of the adsorbent type, Cr(VI) adsorption experiments were conducted using three types of adsorbents (CL, CB200, and FeCB200). Experiments were conducted in two doses to confirm the effect of the adsorbent dose on the change in Cr(VI) adsorption efficiency. Briefly, 1 or 5 g L^{-1} of the adsorbents and 100 mg L^{-1} of Cr(VI) solution were added to 50-mL conical tubes at pH=2. The samples were allowed to adsorb Cr(VI) in a shaker at 25 °C and 150 rpm for 24 h, and filtered using 0.2-μm syringe filters (25HP020AN, Advantec, Japan). The amount of Cr(VI) remaining in the samples after adsorption was determined using a UV-vis spectrophotometer at 540 nm via the diphenylcarbazide method [27]. Adsorption kinetic experiments were performed by varying the adsorption times (5, 10, 20, 40, 60, 180, 300, 600, 900, 1,200, and 1,440 min), and adsorption isotherm experiments were performed with different concentration of the Cr(VI) solution (50 to 500 mg L^{-1}). For the real wastewater application experiments, 100 mg L^{-1} of Cr(VI) was prepared by spiking Cr(VI) into a real wastewater sample and used. All experiments were conducted three times.

5. Adsorption Models

Three kinetic models, pseudo-first-order (Eq. (1)), pseudo-second-order (Eq. (2)), and intra-particle diffusion (Eq. (3)), are applied to fit the adsorption kinetics results as follows [28]:

$$q_t = q_e(1-e^{-k_1 t}), \tag{1}$$

$$q_t = \frac{k_2 q_e^2 t}{1+k_2 q_e t}, \tag{2}$$

$$q_t = k_{id} t^{0.5} + C \tag{3}$$

where q_t is the amount of Cr(VI) adsorbed at time t, and k_1, k_2, and k_{id} are the pseudo-first-order, pseudo-second-order, and intra-particle diffusion rate constants, respectively; C is the boundary layer influence constant in the intra-particle diffusion.

Langmuir (Eq. (4)), Freundlich (Eq. (5)), and Redlich-Peterson (Eq. (6)) isotherm models are applied in the following forms to interpret the experimental results [28]:

$$q_e = \frac{q_m K_L C_e}{1+K_L C_e}, \tag{4}$$

$$q_e = K_F C_e^{1/n}, \tag{5}$$

$$q_e = \frac{K_R C_e}{1+a_R C_e^{g}} \tag{6}$$

where C_e is the equilibrium concentration of Cr(VI) in the aqueous solution; q_m is the maximum Cr(VI) adsorption capacity, K_L is the Langmuir constant related to the affinity of the binding site, and K_F and 1/n are the Freundlich constants related to the adsorption capacity and intensity, respectively; K_R and a_R are the Redlich-

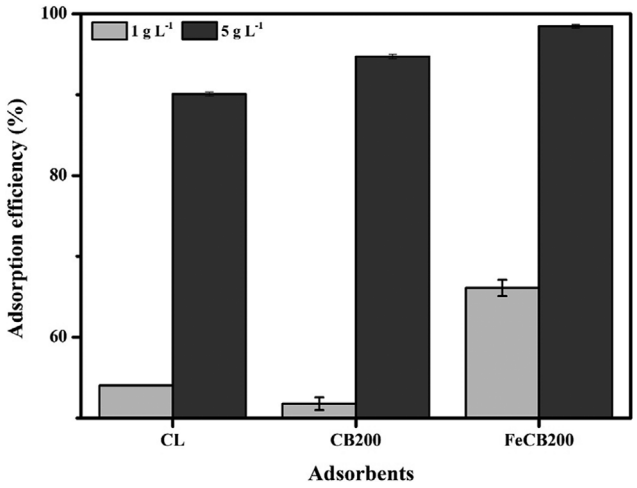

Fig. 1. Adsorption efficiency of different adsorbents for Cr(VI) (Initial concentration=100 mg L^{-1}; pH=2; Temperature=25 °C; Dose=1 g L^{-1} and 5 g L^{-1}; Time=24 h).

Peterson constants related to the adsorption capacity and the affinity of the binding site, respectively; and g is the Redlich-Peterson constant related to the adsorption intensity.

RESULTS AND DISCUSSION

1. Effect of the Type of Adsorbents on Cr(VI) Adsorption

The Cr(VI) adsorption performance of the three *chlorella*-based adsorbents (CL, CB200, and FeCB200) is compared in Fig. 1. The adsorption efficiency of CL, CB200, and FeCB200 at 1 g L^{-1} was 54.05±0.00, 51.80±0.78, 66.12±1.01%, respectively, and 90.09±0.26, 94.74±0.26, and 98.48±0.22%, respectively, at 5 g L^{-1}. Additionally, the removal rates at 5 g L^{-1} were higher than those at 1 g L^{-1}. This can be explained by the rise in the number of active sites on the adsorbent surface, which corresponds to an increase in the adsorbent quantity. As a result, the capacity for adsorbing pollutants also increases [29]. In addition, the Cr(VI) removal rates of the $FeCl_3$-modified adsorbent were higher than those without $FeCl_3$ modification, and FeCB200 exhibited the highest Cr(VI) removal rates. The reason behind this can be ascribed to the augmentation of the adsorbent's specific surface area through chemical modification, leading to the creation of additional reactive sites [30]. Based on the results, FeCB200 with the highest Cr(VI) adsorption efficiency was selected as the optimal adsorbent, and characterization and adsorption experiments were performed.

2. Characterization of FeCB200

The surface characteristics of FeCB200 were examined through SEM and TEM analysis, allowing for observations of its surface morphology (Fig. 2(a)-(b)). The SEM image confirmed the distribution of iron particles on the surface of the FeCB200 adsorbent, and these particles aggregated and covered the surface of the biochar (Fig. 2(a)). This phenomenon can be explained by the inclination of transition metals, such as iron, to form clusters or aggregates on the surface of composites [31,32]. The TEM image revealed that FeCB200 exhibited a micron size and a laminated structure (Fig. 2(b)). The laminated structure was composed of irregular plates, which observation aligns with findings from prior studies [33,34].

The specific surface area of FeCB200 was assessed utilizing the BET analysis, while the pore size distribution was determined using the Barrett-Joyner-Halenda (BJH) method (Table 1 and Fig. 3(a)-

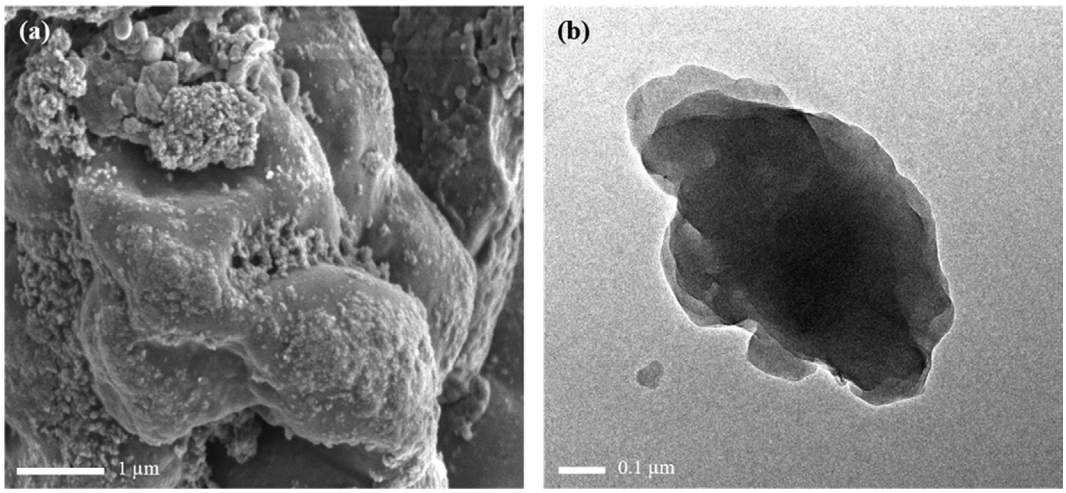

Fig. 2. (a) Scanning electron microscopy (SEM) and (b) Transmission electron microscopy (TEM) images of $FeCl_3$-modified *chlorella*-based biochar (FeCB200).

Table 1. Pore size, specific surface area, pore volume, and pore diameter of FeCB200

Adsorbent	Specific surface area (m^2 g^{-1})	Total pore volume (cm^3 g^{-1})	Average pore diameter (nm)
FeCB200	12.25	0.043	14.06

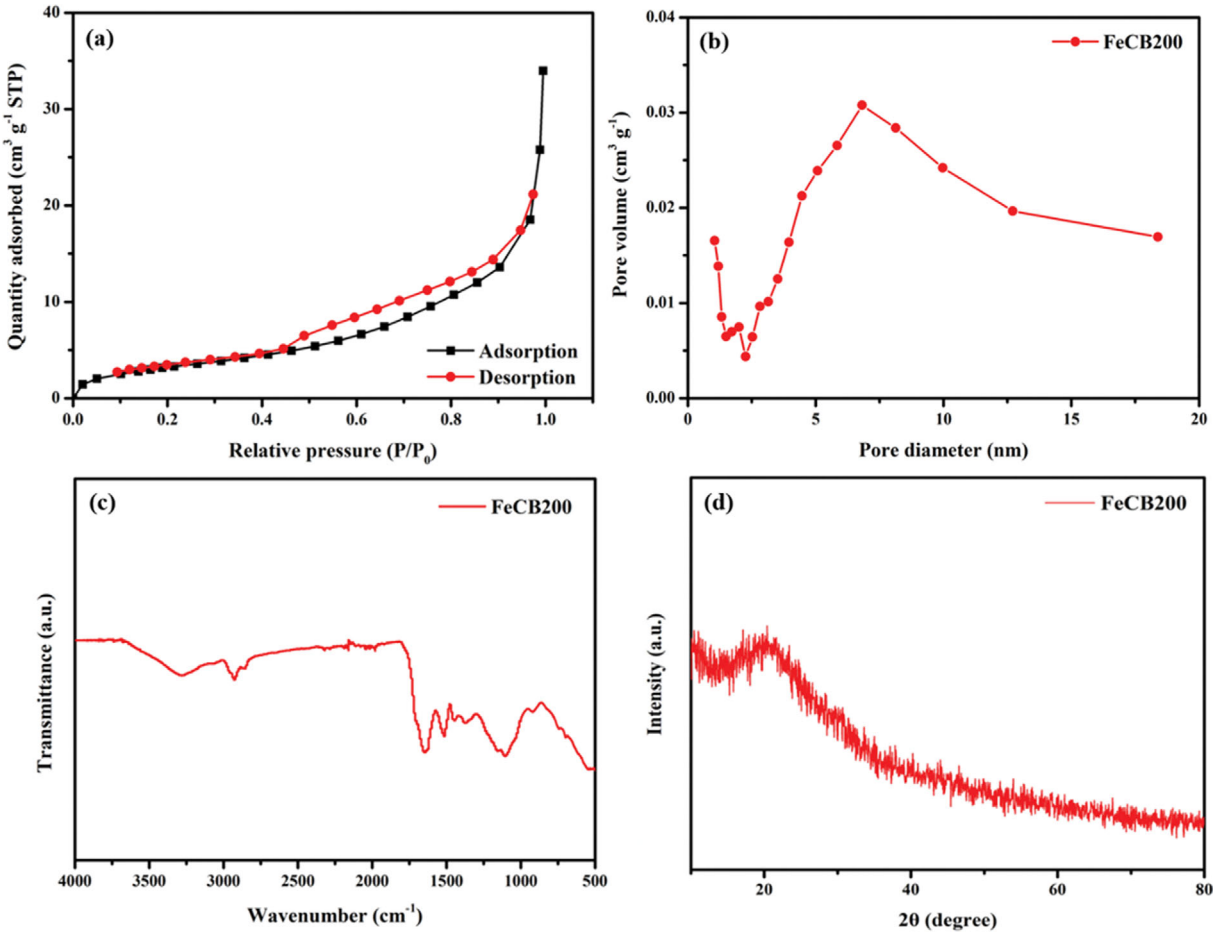

Fig. 3. (a) N_2 adsorption-desorption isotherm, (b) Pore size distribution, (c) Fourier transform infrared (FT-IR) spectra, and (d) X-ray diffraction (XRD) spectra of FeCB200.

(b)). The FeCB200 adsorbent exhibited a type IV N_2 adsorption-desorption isotherm (Fig. 3(a)) with a distinct hysteresis loop [35]. Meanwhile, FeCB200 exhibited a specific surface area of 12.25 m^2 g^{-1} and a total pore volume of 0.043 cm^3 g^{-1} (Table 1). As shown in Fig. 3(b), the pore distribution mainly developed at 7 nm and the average pore length was 14.06 nm; thus, FeCB200 can be considered to be mesoporous. Considering that the specific surface areas of raw *chlorella* and non-modified *chlorella*-based biochar were 0.01-0.28 m^2 g^{-1} and 0.05-2.9 m^2 g^{-1}, respectively, in previous studies [36,37], the specific surface area of biochar modified with $FeCl_3$ was greatly improved. This means that FeCB200 can have more adsorption active sites, i.e., the higher Cr(VI) adsorption efficiency of FeCB200 can be attributed to the enhanced adsorption sites together with the improved surface area.

FT-IR analysis was performed in the wavenumber range of 500-4,000 cm^{-1} to confirm the functional groups present on the surface of FeCB200 (Fig. 3(c)). The characteristic peaks of O-H (3,280 cm^{-1}), aliphatic C-H (2,930 cm^{-1}), C=O (1,630 cm^{-1}), C-H (1,370 cm^{-1}), and C-O (1,150 cm^{-1}) [12,38-41] were observed in the FT-IR spectrum of FeCB200. These were similar to the FTIR spectrum of non-modified *chlorella*-based biochar in previous studies [36,37], confirming that the $FeCl_3$ modification did not have a significant effect on the changes in the functional groups of the biochar in our experimental conditions. The crystalline structure of FeCB200 was determined using XRD analysis (Fig. 3(d)). No crystalline peaks were observed in the XRD pattern of the adsorbent, indicating that the iron particles present in the adsorbent were amorphous. A comparable outcome was documented in a prior study, in which no crystalline peak was identified in the XRD pattern of iron particles [42].

3. Cr(VI)-adsorption Behavior of FeCB200

3-1. Adsorption Kinetics

The adsorption kinetics of the adsorbents were fitted using pseudo-first, pseudo-second order, as well as the intra-particle diffusion model (Table 2 and Fig. 4). A comparison of the R^2 values of the models revealed that the pseudo-second-order model exhibited more enhanced fitting performance than the pseudo-first-order model (R^2=0.865 (1 g L^{-1}); R^2=0.973 (5 g L^{-1})). This indicated that the adsorption of Cr(VI) by FeCB200 was via chemisorption [43]. As demonstrated in Fig. 4(a)-(b), Cr(VI) adsorption by FeCB200 reached equilibrium after 10 h (56.39±0.17%) at 1 g L^{-1} and 1 h (78.49±0.34%) at 5 g L^{-1}. With an increase in the amount of the adsorbent, the number of adsorbable sites for Cr(VI) and the adsorption rate increased [44]. However, the equilibrium adsorption capacity decreased (q_e=56.29 mg g^{-1} (1 g L^{-1}); q_e=18.91 mg g^{-1} (5 g L^{-1})) (Table 2).

When fitted using the intra-particle diffusion model, the adsorp-

Table 2. Parameters of the pseudo-first-order and pseudo-second-order kinetic models for Cr(VI) adsorption on FeCB200

Kinetic models		FeCB200 (1 g L^{-1})	FeCB200 (5 g L^{-1})
Pseudo-first-order	q_e (mg g^{-1})	52.19	18.03
	k_1 (min^{-1})	0.017	0.033
	R^2	0.808	0.950
Pseudo-second-order	q_e (mg g^{-1})	56.29	18.91
	k_2 (mg g^{-1} min^{-1})	0.0004	0.003
	R^2	0.865	0.973
Intra-particle diffusion	k_{i1} (mg g^{-1} $min^{-0.5}$)	1.35	1.19
	C_1 (mg g^{-1})	17.29	3.22
	R^2	0.958	0.970
	k_{i2} (mg g^{-1} $min^{-0.5}$)	0.143	0.142
	C_2 (mg g^{-1})	53.56	14.56
	R^2	0.472	0.981
	k_{i3} (mg g^{-1} $min^{-0.5}$)	-	0.036
	C_3 (mg g^{-1})	-	17.71
	R^2	-	0.302

tion proceeded in two steps for 1 g L^{-1} and three steps for 5 g L^{-1} (Fig. 4(c)-(d)). The first step was the adsorption of Cr(VI) onto the external surface of the adsorbent [45]. Thereafter, the number of adsorption sites decreased as Cr(VI) diffused from the surface of the adsorbent into the particles, stabilizing, and reaching equilibrium [46]. As shown in Table 2, the k value decreased as the steps progress ($k_{i1}>k_{i2}$ (1 g L^{-1}); $k_{i1}>k_{i2}>k_{i3}$ (5 g L^{-1})), indicating that the adsorption of Cr(VI) by FeCB200 was based on a surface or intra-particle diffusion reaction [47,48].

3-2. Adsorption Isotherms

Fig. 5 shows the adsorption isotherms for the Cr(VI) adsorption of FeCB200. In all cases, the adsorption capacity increased as the concentration of Cr(VI) increased. This is because the equilibrium adsorption capacity (q_e) increased as the driving force between pollutant and adsorbent increased [49]. In addition, the number of adsorption sites increased with an increase in the dose of the adsorbent, so equilibrium concentration of Cr(VI) (C_e) and equilibrium adsorption capacity (q_e) decreased [50].

Adsorption isotherms were analyzed by fitting them to models including Langmuir, Freundlich, and Redlich-Peterson models (Table 3 and Fig. 5). The Langmuir model is grounded on the concept of

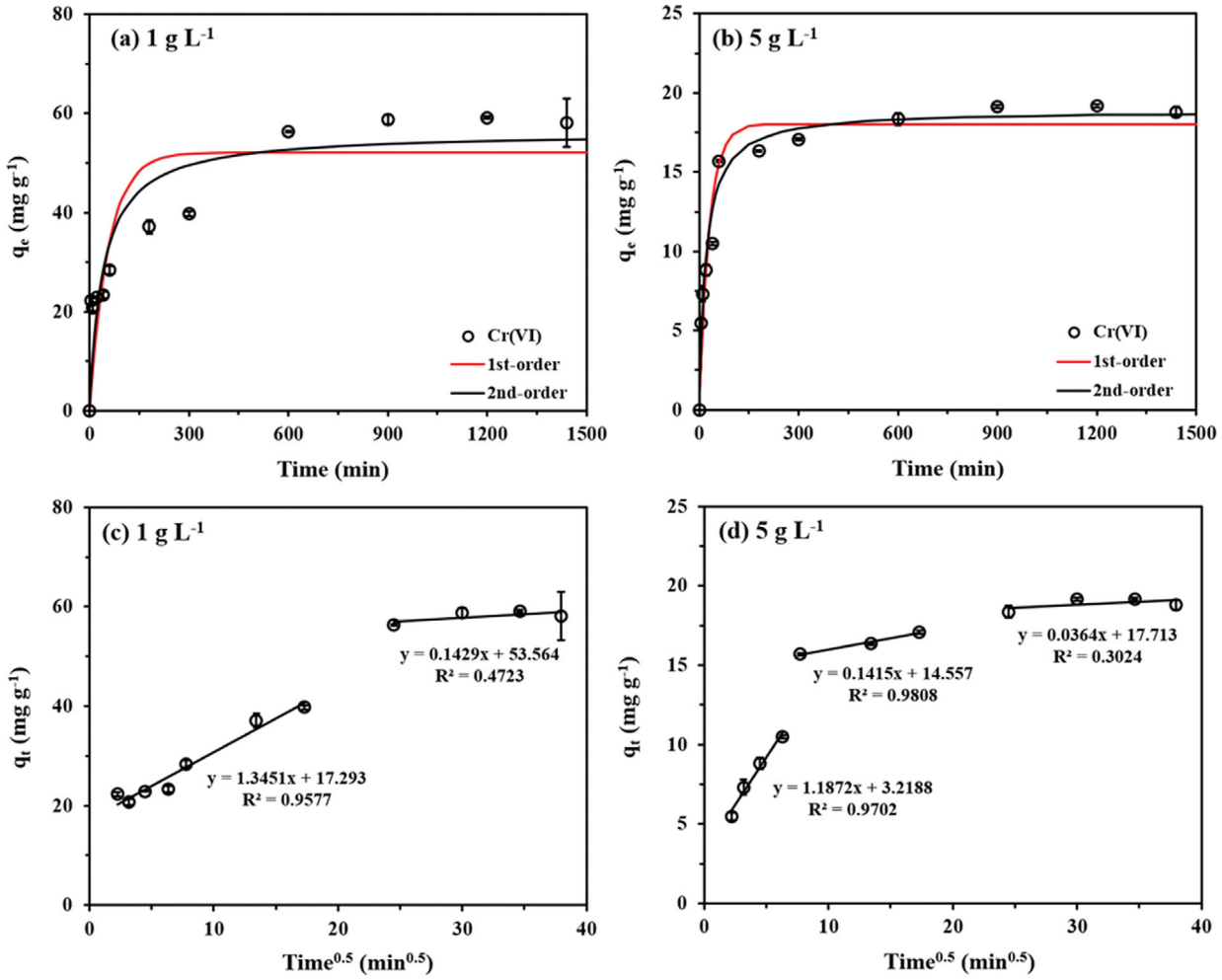

Fig. 4. Adsorption kinetics of FeCB200 fitted using the Pseudo-first-order and Pseudo-second-order models for a dose of (a) 1 g L^{-1} and (b) 5 g L^{-1}; Adsorption kinetics of FeCB200 fitted using the intra-particle diffusion model for a dose of (c) 1 g L^{-1} and (d) 5 g L^{-1}.

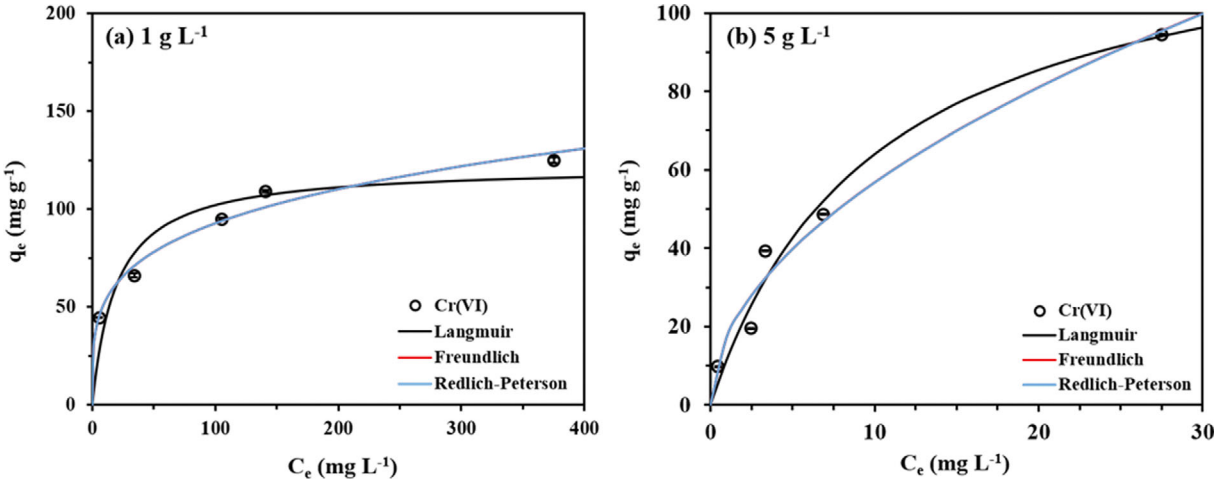

Fig. 5. Adsorption isotherms of FeCB200 fitted using the Freundlich, Langmuir, and Redlich-Peterson models for a dose of (a) 1 g L^{-1} and (b) 5 g L^{-1}.

Table 3. Parameters of the Freundlich, Langmuir, and Redlich-Peterson isotherm models for Cr(VI) adsorption on FeCB200

Isotherm models		FeCB200 (1 g L^{-1})	FeCB200 (5 g L^{-1})
Freundlich	K_F (L mg^{-1})	29.50	17.35
	n^{-1}	0.249	0.514
	R^2	0.975	0.972
Langmuir	q_m (mg g^{-1})	122.16	128.57
	K_L (L mg^{-1})	0.051	0.099
	R^2	0.891	0.974
Redlich-Peterson	K_R (L g^{-1})	202,827.20	154,055.10
	a_R (L mg^{-1})	6,874.99	8,879.59
	g	0.751	0.486
	R^2	0.975	0.972

monolayer adsorption, while the Freundlich model is based on the notion of multilayer adsorption [51,52]. For 1 g L^{-1} dose, the Freundlich model (R^2=0.975) exhibited improved fitting accuracy over the Langmuir model, whereas the Langmuir model exhibited more improved fitting accuracy than the Freundlich model for the 5 g L^{-1} dose (R^2=0.974). Redlich-Peterson is a hybrid model, in which the Freundlich and Langmuir models are combined [53]. This model described the adsorption isotherms well in all cases (R^2>0.972). The adsorption difficulty can be predicted through the n^{-1} value of the Freundlich model and R_L value of the Langmuir model (Eq. (1)) [54]. The calculated n^{-1} (0.249-0.514) and R_L (0.020-0.282) were both between 0 and 1, indicating favorable adsorption of Cr(VI) on FeCB200 [27,54].

$$R_L = (1 + K_L C_0)^{-1} \quad (7)$$

Table 4 shows the comparison of the maximum Cr(VI) adsorption capacity (q_m) on various $FeCl_3$-modified biochars reported in previous studies. The q_m of FeCB200 was found to be higher than other adsorbents (47.46-95.23 mg g^{-1} (previous studies); 122.16-128.57 mg g^{-1} (This study)) compared to other adsorbents. Thus, FeCB200 can be considered as an economical and efficient adsorbent for Cr(VI) removal.

4. Application to Real Wastewater

A real wastewater application experiment was performed to investigate the effect of coexisting substances present in real wastewater on the removal of pollutants. The results of the characteristics analysis of wastewater are shown in Table 5. Cr(VI) was spiked into the final effluent obtained from a wastewater treatment plant, and was adsorbed with FeCB200. As displayed in Fig. 6, the Cr(VI)-

Table 4. Comparison of maximum Cr(VI) adsorption capacity on various $FeCl_3$-modified biochar reported in previous studies

Biomass	Pyrolysis temperature (°C)	Initial concentration (mg L^{-1})	pH	Dose (g L^{-1})	q_m (mg g^{-1})	Reference
Peanut hull	650	10-360	5.13	2	77.54	[56]
Lotus stem	500	10-70	5.4	1.6	26.16	[24]
Enteromorpha prolifera	600	50-500	5.03	2	88.17	[12]
Enteromorpha prolifera	400	100-500	-	1	86.94	[57]
	800				95.23	
Sewage sludge	600	5-25	1	0.4	47.46	[58]
Chlorella	200	50-500	2	1	122.16	This study
				5	128.57	

Table 5. Effluent wastewater characteristic analysis

pH (-)	DOC[a] (mg L^{-1})	UV_{254}[b] (-)	SUVA[c] (-)
7.35±0.01	13.36±1.53	0.059±0.000	0.44

[a]DOC: dissolved organic carbon
[b]UV_{254}: ultraviolet (UV) absorbance at 254 nm
[c]SUVA: specific UV absorbance

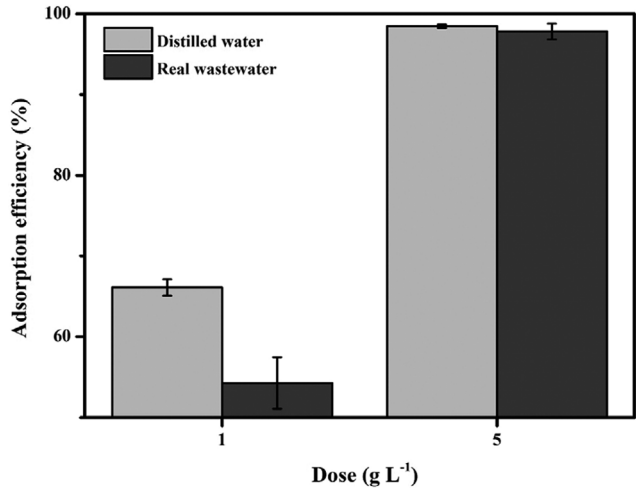

Fig. 6. Real wastewater adsorption of Cr(VI) on FeCB200 (Initial concentration=100 mg L^{-1}; pH=2; Temperature=25 °C; Dose= 1 g L^{-1} and 5 g L^{-1}; Time=24 h).

removal rate at an adsorbent dose of 1 and 5 g L^{-1} was 54.27±3.19 and 97.83±0.99%, respectively. The removal rate (1 g L^{-1}=66.12± 1.01%; 5 g L^{-1}=98.48±0.22%) was reduced compared to the previous. This can be attributed to the organic materials present in the wastewater (DOC=13.36±1.53 mg L^{-1}; UV_{254}=0.059±0.000; SUVA= 0.44), which competed with Cr(VI) at the adsorption sites, and affected the adsorption efficiency of FeCB200 [55]. Nevertheless, the adsorption efficiency of the adsorbent for Cr(VI) was high even in real wastewater.

CONCLUSIONS

An adsorbent based on *chlorella* was prepared and modified with $FeCl_3$. The comparison of the raw biomass, biochar, and $FeCl_3$-modified biochar (CL, CB200, and FeCB200) revealed that FeCB200 exhibited the highest Cr(VI)-adsorption efficiency; thus, FeCB200 was selected as the optimal adsorbent. The investigations on adsorption kinetics demonstrated that the pseudo-second-order model exhibited the highest level of accuracy and best fit for the data. Additionally, the Redlich-Peterson model, a hybrid model, exhibited good fitting accuracy (R^2>0.972) for the adsorption isotherms, but there was a difference according to the dose of the adsorbent. Further, although it exhibited high efficiency, the organic matter present in real wastewater decreased the Cr(VI)-removal efficiency of FeCB200. These results indicate the potential application of *chlorella*-based $FeCl_3$-modified biochar adsorbent as an effective solution for the removal of Cr(VI) from water environments, highlighting its capability as a promising adsorbent.

ACKNOWLEDGEMENTS

This work was supported by R&D Project of the Korea Mine Rehabilitation and Mineral Resources Corporation in 2023.

REFERENCES

1. W. S. Chai, J. Y. Cheun, P. S. Kumar, M. Mubashir, Z. Majeed, F. Banat, S.-H. Ho and P. L. Show, *J. Clean. Prod.*, **296**, 126589 (2021).
2. A. E. Burakov, E. V. Galunin, I. V. Burakova, A. E. Kucherova, S. Agarwal, A. G. Tkachev and V. K. Gupta, *Ecotoxicol. Environ. Saf.*, **148**, 702 (2018).
3. Y.-J. Lee, C.-Y. Son, C.-G. Lee, Y. J. Jeong, I. S. Cho, S.-J. Park and J. Lee, *Alexandria Eng. J.*, **75**, 151 (2023).
4. X. Wang, J. Xu, J. Liu, J. Liu, F. Xia, C. Wang, R. A. Dahlgren and W. Liu, *Sci. Total Environ.*, **700**, 134414 (2020).
5. C.-G. Lee, J.-A. Park, J.-W. Choi, S.-O. Ko and S.-H. Lee, *Water, Air, Soil Pollut.*, **227**(8) (2016).
6. M. Xu, X. Ma, Y. Chen, L. Hu, B. Wang and M. Qiu, *J. Mol. Liq.*, **366**, 120262 (2022).
7. G. Lian, B. Wang, X. Lee, L. Li, T. Liu and W. Lyu, *Sci. Total Environ.*, **697**, 134119 (2019).
8. Z. Fan, Q. Zhang, B. Gao, M. Li, C. Liu and Y. Qiu, *Chemosphere*, **217**, 85 (2019).
9. Y. Ren, Y. Han, X. Lei, C. Lu, J. Liu, G. Zhang, B. Zhang and Q. Zhang, *Colloids Surf. A: Physicochem. Eng. Asp.*, **604**, 125279 (2020).
10. L. Li, J. Zhang, Y. Li and C. Yang, *J. Membr. Sci.*, **544**, 333 (2017).
11. Y. Yi, X. Wang, J. Ma and P. Ning, *Environ. Res.*, **189**, 109912 (2020).
12. Y. Chen, B. Wang, J. Xin, P. Sun and D. Wu, *Ecotoxicol. Environ. Saf.*, **164**, 440 (2018).
13. S. Karthick, R. Palani, D. Sivakumar and N. Meyyappan, *Membr. Water Treatment*, **13**(5), 209 (2022).
14. J. H. Park, Y. S. Ok, S. H. Kim, J. S. Cho, J. S. Heo, R. D. Delaune and D. C. Seo, *Chemosphere*, **142**, 77 (2016).
15. B. Qiu, X. Tao, H. Wang, W. Li, X. Ding and H. Chu, *J. Anal. Appl. Pyrolysis*, **155**, 105081 (2021).
16. J. Xu, Y. Yin, Z. Tan, B. Wang, X. Guo, X. Li and J. Liu, *J. Environ. Sci. (China)*, **78**, 109 (2019).
17. A. A. Khan, J. Gul, S. R. Naqvi, I. Ali, W. Farooq, R. Liaqat, H. AlMohamadi, L. Stepanec and D. Juchelkova, *Chemosphere*, **306**, 135565 (2022).
18. X. Jiang, X. Yin, Y. Tian, S. Zhang, Y. Liu, Z. Deng, Y. Lin and L. Wang, *Sci. Total Environ.*, **813**, 152488 (2022).
19. M. Yadav, V. Kumar, N. Sandal and M. K. Chauhan, *J. Appl. Phycol.*, **34**(6), 2743 (2022).
20. A. M. Lizzul, A. Lekuona-Amundarain, S. Purton and L. C. Campos, *Biology (Basel)*, **7**(2), 25 (2018).
21. J. Qu, Y. Wang, X. Tian, Z. Jiang, F. Deng, Y. Tao, Q. Jiang, L. Wang and Y. Zhang, *J. Hazard. Mater.*, **401**, 123292 (2021).
22. H. Zeng, H. Zeng, H. Zhang, A. Shahab, K. Zhang, Y. Lu, I. Nabi, F. Naseem and H. Ullah, *J. Clean. Prod.*, **286**, 124964 (2021).
23. Y. Luo, L. Zeng, Y. Zhao, Z. Zhao, M. Wei, B. Jiang, J. Fan and D. Li, *J. Water Process Eng.*, **47**, 102743 (2022).
24. Z. Feng, N. Chen, C. Feng and Y. Gao, *Colloids Surf. A: Physicochem.*

Eng. Asp., **551**, 17 (2018).
25. D. Patwa, U. Bordoloi, A. A. Dubey, K. Ravi, S. Sekharan and P. Kalita, *Sci. Total Environ.*, **833**, 155253 (2022).
26. M. Ahmad, A. U. Rajapaksha, J. E. Lim, M. Zhang, N. Bolan, D. Mohan, M. Vithanage, S. S. Lee and Y. S. Ok, *Chemosphere*, **99**, 19 (2014).
27. X. Zhang, L. Lv, Y. Qin, M. Xu, X. Jia and Z. Chen, *Bioresour. Technol.*, **256**, 1 (2018).
28. Y.-J. Lee, J.-I. Lee, C.-G. Lee and S.-J. Park, *Membr. Water Treatment*, **14**(1), 1 (2023).
29. S. Rangabhashiyam and P. Balasubramanian, *Bioresour. Technol. Rep.*, **5**, 261 (2019).
30. F. X. Dong, L. Yan, X. H. Zhou, S. T. Huang, J. Y. Liang, W. X. Zhang, Z. W. Guo, P. R. Guo, W. Qian, L. J. Kong, W. Chu and Z. H. Diao, *J. Hazard. Mater.*, **416**, 125930 (2021).
31. J.-H. Chu, J.-K. Kang, S.-J. Park and C.-G. Lee, *J. Water Process Eng.*, **37**, 101455 (2020).
32. A. Ateş and K. O. Oskay, *Surf. Interfaces*, **29**, 101733 (2022).
33. H. Fu, S. Ma, P. Zhao, S. Xu and S. Zhan, *Chem. Eng. J.,* **360**, 157 (2019).
34. A. Shan, A. Idrees, W. Q. Zaman, Z. Abbas, M. Ali, M. S. U. Rehman, S. Hussain, M. Danish, X. Gu and S. Lyu, *J. Environ. Chem. Eng.*, **9**(1), 104808 (2021).
35. X. Li, J. Xu, X. Luo and J. Shi, *Bioresour. Technol.*, **360**, 127526 (2022).
36. F. Sotoudehniakarani, A. Alayat and A. G. McDonald, *J. Anal. Appl. Pyrolysis*, **139**, 258 (2019).
37. Z. Yang, J. Hou, J. Wu and L. Miao, *Ecotoxicol. Environ. Saf.*, **225**, 112750 (2021).
38. K. Govindaraju, R. Vinu, R. Gautam, R. Vasantharaja, M. Niranjan and I. Sundar, *Biomass Conv. Biorefinery* (2022).
39. J. S. Lazarotto, K. da Boit Martinello, J. Georgin, D. S. P. Franco, M. S. Netto, D. G. A. Piccilli, L. F. O. Silva, E. C. Lima and G. L. Dotto, *Chem. Eng. Res. Des.*, **180**, 67 (2022).
40. Z. Xu, Z. Sun, Y. Zhou, W. Chen, T. Zhang, Y. Huang, D. Zhang, *Colloids Surf. A: Physicochem. Eng. Asp.*, **582**, 123934 (2019).
41. Y. Cui, A. Masud, N. Aich and J. D. Atkinson, *J. Hazard. Mater.*, **368**, 477 (2019).
42. S. Rawat, K. Samreen, A. K. Nayak, J. Singh and J. R. Koduru, *Environ. Nanotechnol., Monitoring Manag.*, **15**, 100426 (2021).
43. F. Yang, Y. Jiang, M. Dai, X. Hou and C. Peng, *J. Hazard. Mater.*, **424**(Pt C), 127542 (2022).
44. Y. Wei, S. Wei, C. Liu, T. Chen, Y. Tang, J. Ma, K. Yin and S. Luo, *Water Res.*, **167**, 115107 (2019).
45. Y. Yi, X. Wang, J. Ma and P. Ning, *Powder Technol.*, **388**, 485 (2021).
46. S. Sun, X. Zeng, Y. Gao, W. Zhang, L. Zhou, X. Zeng, W. Liu, Q. Jiang, C. Jiang and S. Wang, *J. Clean. Prod.*, **317**, 128412 (2021).
47. L. Yan, F.-X. Dong, X. Lin, X.-H. Zhou, L.-J. Kong, W. Chu and Z.-H. Diao, *Environ. Technol. Innov.*, **24**, 102057 (2021).
48. L. Yan, F.-X. Dong, Y. Li, P.-R. Guo, L.-J. Kong, W. Chu and Z.-H. Diao, *J. Environ. Chem. Eng.*, **10**(2), 107396 (2022).
49. S. Moon, J. Ryu, J. Hwang and C. G. Lee, *Chemosphere*, **313**, 137448 (2023).
50. A. A. Lawal, M. A. Hassan, M. A. Ahmad Farid, T. A. Tengku Yasim-Anuar, M. H. Samsudin, M. Z. Mohd Yusoff, M. R. Zakaria, M. N. Mokhtar and Y. Shirai, *Environ. Pollut.*, **269**, 116197 (2021).
51. S. Shi, J. Yang, S. Liang, M. Li, Q. Gan, K. Xiao and J. Hu, *Sci. Total Environ.*, **628-629**, 499 (2018).
52. A. Kumar Prajapati and M. Kumar Mondal, *J. Mol. Liq.*, **349**, 118161 (2022).
53. Z. Wan, D. W. Cho, D. C. W. Tsang, M. Li, T. Sun and F. Verpoort, *Environ. Pollut.*, **247**, 410 (2019).
54. Y. Cheng, B. Wang, J. Shen, P. Yan, J. Kang, W. Wang, L. Bi, X. Zhu, Y. Li, S. Wang, L. Shen and Z. Chen, *J. Hazard. Mater.*, **432**, 128757 (2022).
55. L. Min, Z. Zhongsheng, L. Zhe and W. Haitao, *Ecol. Eng.*, **149**, 105792 (2020).
56. Y. Han, X. Cao, X. Ouyang, S. P. Sohi and J. Chen, *Chemosphere*, **145**, 336 (2016).
57. Y. Wang, Q. Yang, J. Chen, J. Yang, Y. Zhang, Y. Chen, X. Li, W. Du, A. Liang, S. H. Ho and J. S. Chang, *J. Hazard. Mater.*, **395**, 122658 (2020).
58. C. Shen, L. Gu, S. Chen, Y. Jiang, P. Huang, H. Li, H. Yu and D. Xia, *J. Environ. Chem. Eng.*, **10**(6), 108575 (2022).